Impact Quantification of Wide-Base Tire Loading on Secondary Road Flexible Pavements

Hao Wang, A.M.ASCE[1]; and Imad L. Al-Qadi, Dist.M.ASCE[2]

Abstract: There is a need to evaluate the damage caused by the new generation of wide-base tires on low-volume secondary roads because of their increased use on trucks. In this study, a three-dimensional (3D) finite-element (FE) model was built to simulate the realistic tire loading on secondary road pavements. The model allows for predicting pavement responses to loading applied by various tire configurations. In addition, the model incorporates the measured 3D tire-pavement contact stresses, models hot-mix asphalt (HMA) as linear viscoelastic material, simulates continuous moving load, and utilizes implicit dynamic analysis. The analyzed pavement structures comprised a 76-mm HMA layer and an aggregate base layer with various thicknesses (203, 305, and 457 mm). The impact of a wide-base tire on secondary road pavement damage was analyzed using available damage models and was compared to that resulting from conventional dual-tire assemblies. It was found that the new wide-base tire (455/55R22.5) caused greater fatigue damage, subgrade rutting, and HMA rutting (densification) but less HMA rutting (shear) and base shear failure compared to the conventional dual-tire assembly when carrying the same load. The findings indicate that wide-base tires' impact on secondary road pavements depends on the roads' predominant failure mechanisms. Hence, calculated combined damage ratios can be used for road usage pricing and pavement design practice when wide-base tires are used. **DOI: 10.1061/(ASCE)TE.1943-5436.0000245.**

CE Database subject headings: Tires; Highways and roads; Flexible pavements; Finite element method; Damage.

Author keywords: Secondary roads; Flexible pavements; Wide-base tire; Finite-element model; Combined damage ratio.

Background

The trucking industry has, of late, been using wide-base single tires as an alternative to conventional dual-tire assemblies. Compared to the conventional dual-tire assembly, it is reported that wide-base tires improve fuel efficiency, reduce emissions, increase payload, exhibit superior braking and comfort, and reduce tire repair, maintenance, and recycling costs. (Ang-Olson and Schroeer 2002; Al-Qadi and Elsefi 2007). The first generation of wide-base tires (385/65R22.5 and 425/65R22.5) in the early 1980s were found to cause a significant increase in pavement damage compared to dual-tire assemblies. This has led many transportation agencies to discourage their use. For example, the first generation of wide-base tires caused 1.5–2.0 times more rut depth and 2.0–4.0 times more fatigue cracking than a dual-tire assembly when carrying the same load (Huhtala et al. 1989; Bonaquist 1992; Akram et al. 1992; Perdomo and Nokes 1993; Myers et al. 1999; Siddharthan et al. 2002; Kim et al. 2005). The new generation of wide-base tires (445/50R22.5 and 455/55R22.5) came to market in the 2000s to possibly reduce pavement damage and provide other safety and cost-saving advantages. The new generation of wide-base tires are 15–18% wider than the first generation and do not require high tire inflation pressure owing to their special wall design (Al-Qadi et al. 2005). Thus, the impact of the new generation of wide-base tires on pavement damage needs to be investigated.

Results of COST Action 334 (2001) indicated that the new generation of wide-base tires would cause approximately the same primary rutting damage as a dual-tire assembly on primary roads and 44–52% more combined damage (20% primary rutting, 40% secondary rutting, and 40% fatigue cracking) on secondary roads. Al-Qadi et al. (2002, 2005) concluded that the new wide-base tires caused slightly more fatigue damage and less primary rutting damage than a dual-tire assembly, based on the comprehensive experimental and theoretical studies conducted at the Virginia Smart Road. Pierre et al. (2003) conducted field measrements and found that the wide-base 455/55R22.5 tire caused more distortions at the pavement base in the spring and similar distortions in the summer, compared to the dual tires. The wide-base 455/55R22.5 tire was also found to cause less primary rutting than the dual tires. Priest et al. (2005) conducted a study at the NCAT Test Track in Auburn, Alabama, and concluded that the new wide-base tire (445/50R22.5) resulted in a similar pavement fatigue life as the standard dual-tire assembly (275/80R22.5). Al-Qadi and Wang (2009a) found that the new wide-base tire (455/55R22.5) induced greater fatigue damage but similar or less near-surface cracking and hot-mix asphalt (HMA) rutting (shear flow) potential in perpetual pavements when compared to dual-tire assemblies. These studies indicate that the impact of wide-base tires on pavement damage depends on pavement structure, the pavement failure mechanism considered, and environmental conditions.

The predominant failure mechanisms of secondary roads are different from those of primary roads or interstate highways. Although previous research has achieved significant advances,

[1]Assistant Professor, Dept. of Civil and Environmental Engineering, Rutgers Univ., Piscataway, NJ 08854 (corresponding author). E-mail: hwang.cee@rutgers.edu; formerly, Graduate Research Assistant, Dept. of Civil and Environmental Engineering, Univ. of Illinois at Urbana-Champaign, IL 61801

[2]Founder Professor of Engineering and Director, Illinois Center for Transportation, Univ. of Illinois at Urbana-Champaign, IL 61801. E-mail: alqadi@illinois.edu

Note. This manuscript was submitted on January 7, 2010; approved on October 29, 2010; published online on November 24, 2010. Discussion period open until February 1, 2012; separate discussions must be submitted for individual papers. This paper is part of the ***Journal of Transportation Engineering***, Vol. 137, No. 9, September 1, 2011. ©ASCE, ISSN 0733-947X/2011/9-630–639/$25.00.

the new wide-base tires' impact on secondary road pavements has not been thoroughly investigated and quantified. This study, therefore, aimed to quantify the pavement damage on secondary roads caused by various tire configurations. These research findings will help state departments of transportation (DOTs) predict the impact of the new wide-base tires on the road infrastructure and provide the basis for reasonable load regulations and fee charges for trucking operations. The implementation of appropriate fee regulations will ultimately balance economic benefits (for the trucking industry) with pavement repair costs (for state DOTs and other agencies).

Objective and Scope

The main objective of this study was to evaluate the impact of new wide-base tires on secondary road pavements. The conventional pavement design mainly uses the linear layered elastic theory to predict pavement responses under vehicular loading. The layered theory assumes a uniform stress distribution within a circular contact area. Hence, this analytical technique cannot reflect the difference in contact stress distribution patterns between wide-base tires and conventional dual-tire assemblies at the tire-pavement interface. To overcome these limitations, a three-dimensional (3D) finite-element (FE) model was built to simulate the realistic tire loading on secondary road pavements. The model allows for predicting pavement responses to loading applied by various tire configurations. It incorporates measured 3D tire-pavement contact stresses, models HMA as linear viscoelastic material, simulates continuous moving load, and utilizes implicit dynamic analysis.

The analyzed pavement structures were comprised of a 76-mm HMA layer and an unbound aggregate base layer with various thicknesses (203, 305, and 457 mm). The critical pavement responses under various tire configurations at intermediate and high temperatures were calculated and compared. The impact of the new generation of wide-base tire (455/55R22.5) on damage to secondary road pavement was compared to the impact of the conventional dual-tire assembly for the above-mentioned pavement designs. The overall impact of wide-base tires on road usage pricing and pavement design practice was evaluated using the calculated damage ratios.

Tire-Pavement Contact Stress

It has been documented that tire-pavement contact stresses have three components: vertical, transverse, and longitudinal. These 3D tire contact stresses result in a complex stress state near the pavement surface. Drakos et al. (2001) found that the 3D tire contact stresses increased HMA instability rutting potential. De Beer et al. (2002) suggested that responses of thin HMA pavements are sensitive to vertical load shape and distribution. Park et al. (2005) concluded that the nonuniform contact stresses caused highly localized strains that could initiate rutting at the flexible pavement surface. Yoo and Al-Qadi (2008) showed that the vertical shear strain under 3D tire contact stress could be responsible for the development of near-surface cracking. Wang and Al-Qadi (2009) reported that the 3D tire contact stresses induced greater octahedral shear stress at pavement near-surface, compared to uniform contact stress distribution. Thus, it is necessary to define the realistic tire loading condition to accurately predict pavement responses and performances.

Figs. 1(a) and 1(b) show the comparisons of maximum vertical and transverse contact stresses at each rib of the dual-tire assembly and the new wide-base tire (35 kN load and 720 kPa inflation pressure). The contact stresses were measured by the tire manufacturer using three-dimensional load pins at the tire-pavement interface. The tire imprint area includes five ribs for one tire of a dual-tire assembly and nine ribs for the wide-base tire. The maximum vertical stress under the center rib was found to be 1.4–1.6 times the inflation pressure owing to the nonuniform contact stress distribution. However, the wide-base tire has relatively more uniform vertical stress distribution along the tire width compared to the dual-tire assembly. Because the transverse contact stresses are mainly associated with the Poisson's effect of rubber material for radial tires, the transverse contact stresses have a distinct asymmetric distribution beneath each rib. Fig. 1(b) shows the maximum transverse contact stresses under one side of each tire rib; the contact stresses under the other side of each rib have similar magnitudes but in opposite directions. The maximum transverse contact stresses at each rib vary along the tire width for both the dual-tire assembly and wide-base tires. The 455 wide-base tire has lower transverse contact stresses than the dual-tire assembly, especially at the tire's edge ribs. More details about 3D contact stress distributions at the tire-pavement interface can be found elsewhere (Al-Qadi et al. 2008; Yoo and Al-Qadi 2008; Wang and Al-Qadi 2009).

Pavement Structure and Material Characterization

The secondary road pavement structures used in this study resembled those constructed for accelerated pavement testing at the Advanced Transportation Research and Engineering Laboratory (ATREL) at the University of Illinois. More information on construction and instrumentation of these pavement sections is available elsewhere (Al-Qadi et al. 2007). The analyzed pavement structures comprised a 76-mm SM-9.5 (surface mix with maximum nominal aggregate size of 9.5 mm) HMA layer and an unbound

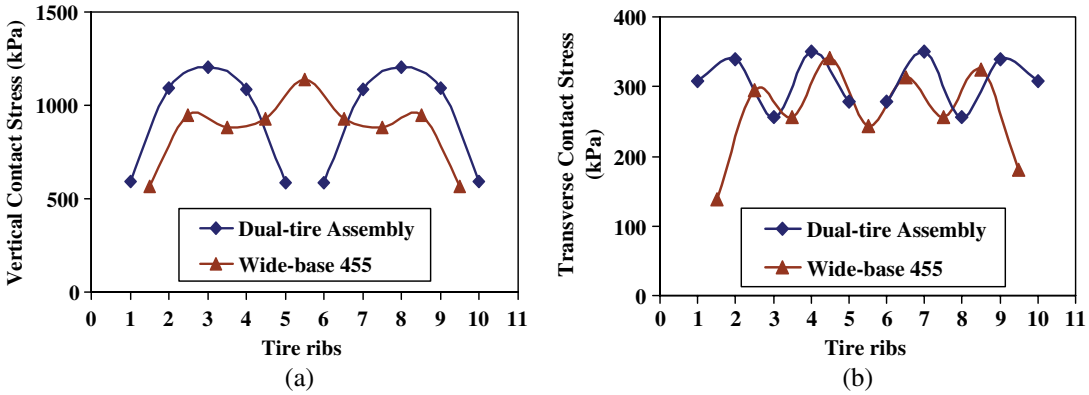

Fig. 1. Comparisons between dual-tire assembly and wide-base tire for: (a) vertical; and (b) transverse contact stresses

aggregate base layer with various thicknesses (203, 305, and 457 mm for sections A, B, and D, respectively). PG 64-22 binder was used in the SM-9.5 mix for the HMA layer. Dense-graded crushed limestone aggregates were used for the base layer. The pavement sections were constructed on subgrade having a low California bearing ratio (CBR) of 4%.

A linear viscoelastic model was used to simulate HMA behavior. The HMA relaxation modulus was converted from laboratory-determined creep compliance test results through an interconversion procedure (Park and Kim 1999). The shear and bulk relaxation moduli were then calculated, assuming a constant Poisson's ratio, and fitted into a Prony series of the generalized Maxwell solid model, Eqs. (1) and (2). The temperature dependency of the HMA modulus was characterized by the time-temperature superposition principle because HMA has been proven to be a thermorheologically simple (TRS) material. The time-temperature shift factor was approximated by the Williams-Landell-Ferry (WLF) function, Eq. (3) (*ABAQUS version 6.7*)

$$G(t) = G_0\left[1 - \sum_{i=1}^{n} G_i(1 - e^{-t/\tau_i})\right] \quad (1)$$

$$K(t) = K_0\left[1 - \sum_{i=1}^{n} K_i(1 - e^{-t/\tau_i})\right] \quad (2)$$

where G = shear modulus; K = bulk modulus; t = reduced relaxation time; G_0 and K_0 = instantaneous shear and volumetric modulus; and G_i, K_i, and τ_i = Prony series parameters

$$\log(a_T) = -\frac{C_1(T - T_0)}{C_2 + (T - T_0)} \quad (3)$$

where $\log(a_T)$ = log of the shift factor; T_0 = reference temperature; T = actual temperature corresponding to the shift factor; and C_1 and C_2 are regression parameters.

The aggregate base and subgrade were assumed as linear elastic material. The resilient modulus of subgrade was estimated from its CBR value using the approach in the 2002 Mechanistic-Empirical Pavement Design Guide (MEPDG) [Applied Research Associates, Inc. (ARA) 2004]. The resilient modulus of the aggregate base was estimated as the average measured modulus from repeated-load triaxial tests at five confining pressure levels (21, 35, 69, 104, and 138 kPa) in accordance with the AASHTO T307 procedure. Table 1 summarizes the material parameters for each pavement layer.

Development of 3D FE Model

The layered elastic theory is usually used to calculate flexible pavement responses to truck loading owing to its simplicity. In comparison to the relatively simple layered elastic theory, the finite-element method (FEM) can be a complex and costly analysis tool. However, the application of FE techniques allows for more accurate simulation of complex material properties and realistic tire loading. Thus, a 3D FE model was built using ABAQUS version 6.7. The 3D FE model is more appropriate, compared to the axisymmetric or two-dimensional (2D) plane model. It can consider the measured 3D tire-pavement contact stress distribution under each rib, as well as the dynamic transient loading associated with a moving vehicle.

Table 1. Material Parameters for Each Pavement Layer

	Elastic modulus (MPa)	Poisson's ratio	Prony series (25°C) G_i or K_i	Prony series (25°C) τ_i	WLF parameters	
HMA layer	9,840	0.35	6.31×10^{-1}	2.06×10^{-2}	C1	18.1
			2.51×10^{-1}	1.73×10^{-1}		
			8.47×10^{-2}	1.29×10^{0}		
			2.67×10^{-2}	5.35×10^{0}	C2	164.7
			6.66×10^{-3}	1.06×10^{2}		
Base	193	0.30		—		
Subgrade	43	0.40		—		

Model Geometry

Since the behavior of a layered pavement system might not be approximated using truss, beam, or shell elements, 3D continuum solid elements are often selected to simulate the problem under consideration. In this study, eight-node linear brick elements with reduced integration (C3D8R) were used for the finite domains, whereas infinite elements (CIN3D8) were used to reduce a large number of far-field elements without significant loss of accuracy and create a "silent" boundary for the dynamic analysis (*ABAQUS version 6.7*). Fig. 2 illustrates the 3D FE model that simulates the pavement sections.

For the FE model, a fine mesh was used around the loading area along the wheel-path, and a relatively coarse mesh was used far away from the loading area. The element horizontal dimensions along the vehicle loading area were dictated by the tire rib and groove geometries. Hence, the length of elements within the loading area was selected to be 15–18 mm in the transverse direction and 20 mm in the longitudinal (traffic) direction. Based on the study by Yoo and Al-Qadi (2008), the element thicknesses were selected to be 9.5 mm for the HMA layers and 20–30 mm for the base layers. To define the infinite boundaries at both sides, as well as the bottom of the FE mesh, a sensitivity analysis was performed. After comparing the transverse and longitudinal stress/strain responses at the bottom of the HMA, the horizontal location of the infinite boundary from the load center needed to be greater than 900 mm to obtain the closest solution to the full-sized reference FE model of $3 \times 3 \times 5$ m. The location of the bottom infinite boundary element was recommended to be at a depth of 1,100 mm, where the maximum compressive stress in the subgrade became insignificant at 1% or less of the maximum tire-pavement contact stress. The final selected model size has an in-plane dimension of 2.1×2.1 m and a vertical dimension of

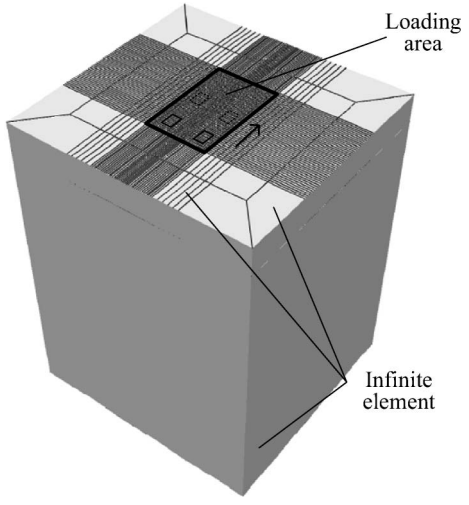

Fig. 2. Illustration of mesh of 3D FE model

2.5 m to achieve the balance between computation cost and accuracy. Only single-axle loading was simulated in this study. Although tandem-axle loading can be simulated in the model, a high computation cost would be required because of the increase in model size.

Simulation of Moving Transient Load

A vehicle load applied on a pavement surface is the sum of the static load and a dynamic tire force. The dynamic tire force is the result of the vehicle's response to the longitudinal unevenness (roughness) of the road surface. To define the dynamic tire force, intensive field measurements from vehicle axles may be needed. To characterize the transient local dynamic load without extensive field data, as in this study, the dynamic loading can be simplified by using the measured loading amplitude within the tire imprint area on a smooth pavement surface.

There are several methods that can be used to simulate the tire loading: stationary constant load; moving constant load; stationary transient load (triangle, trapezoidal, or haversine function); and moving transient load. The load applied by a tire is by nature continuously changing as a vehicle approaches and leaves a location. To simulate the movement of a tire at a certain speed, the concept of a continuously moving load was used. In this approach, the tire loading imprint area is gradually shifted over the pavement surface at each step until a single wheel pass is completed (Fig. 3). For each loading step, linear loading amplitude was applied to accurately simulate the variation of contact stress in the entrance and exit parts of the tire imprint area. The step time was decided by the tire moving speed and element lengths. More details about the continuous moving load approach are available elswhere (Yoo and Al-Qadi 2007).

Incorporation of Tire-Pavement Contact Stress

In the FE model, the measured 3D tire-pavement contact stresses (vertical, transverse, and longitudinal) under each rib were applied, respectively, on the tire imprint area, (Fig. 4). Generally, the tire imprint area of each rib includes two elements laterally and seven to 10 elements longitudinally. The exact footprint shape at a specific load level and tire pressure was considered by adjusting the number and dimension of elements within each rib. All elements along a tire rib were loaded with nonuniform vertical contact stresses corresponding to their locations within the imprint area. The loading amplitudes of vertical contact stresses continuously change at each step as the tire moves. The transverse and longitudinal contact stresses were converted into the equivalent concentrated forces using element shape functions and were assumed constant at each load step. The longitudinal contact stress was applied on the middle nodes of each rib, while the transverse contact stress was applied on the side nodes of each rib.

Implicit Dynamic Analysis

The dynamic transient loading on pavement caused by a moving load is classified as a structure dynamic problem rather than a wave propagation problem, owing to the fact that the vehicle speed is much less than the stress wave propagation speed in the flexible pavement structure (OECD 1992). The dynamic equilibrium equation (Eq. (4)) can be solved by a direct integration method such as using implicit or explicit modes in ABAQUS. Using an implicit method is usually more effective for a structure dynamics problem such as this one (Bathe 1996)

$$[M]\{\ddot{U}\} + [C]\{\dot{U}\} + [K]\{U\} = \{P\} \tag{4}$$

where, $[M]$ = mass matrix; $[C]$ = damping matrix; $[K]$ = stiffness matrix; $\{P\}$ = external force vector; $\{\ddot{U}\}$ = acceleration vector; $\{\dot{U}\}$ = velocity vector; and $\{U\}$ = displacement vector.

In addition, the energy dissipation rules among an arbitrary damping factor, a friction factor, or a viscoelastic material behavior can be defined in the dynamic analysis. In the case of using viscoelastic material behavior for an HMA layer, it is not necessary to introduce additional structural or mass damping rules for that layer. The damping ratio of 5% and the Rayleigh damping scheme were used for the base layer and subgrade (Chopra 2001).

Interface Model

Contact conditions at layer interfaces are also critical parameters that significantly affect pavement responses to vehicular loading. The Coulomb friction model was used at the HMA-base and base-subgrade interfaces. This model assumes that the resistance to movement is proportional to the normal stress at an interface. In this case, the interface may resist movement up to a certain level of shear strength and then interfaces start to slide relative to one another. If the relative motion occurs, the frictional stress will remain constant.

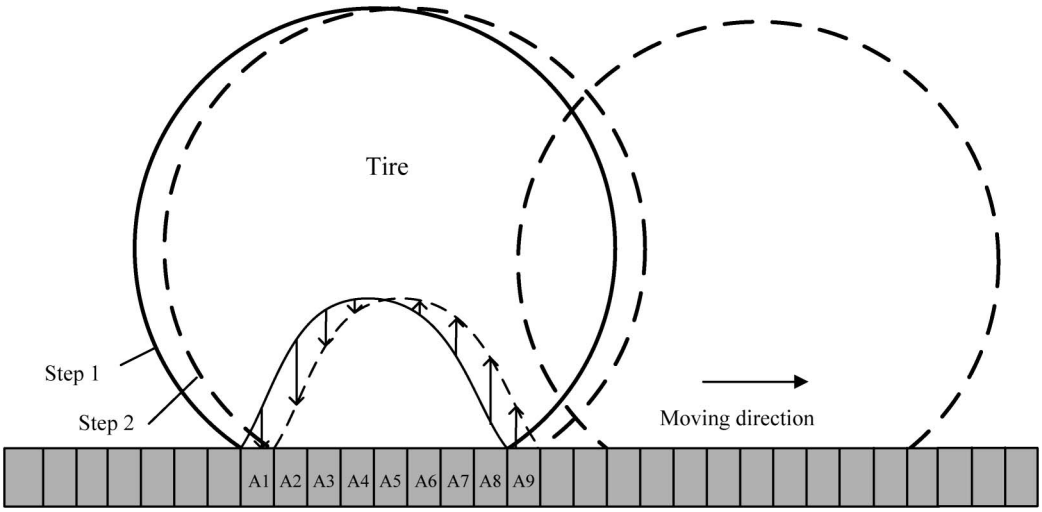

Fig. 3. Schematic illustration of tire moving along pavement surface

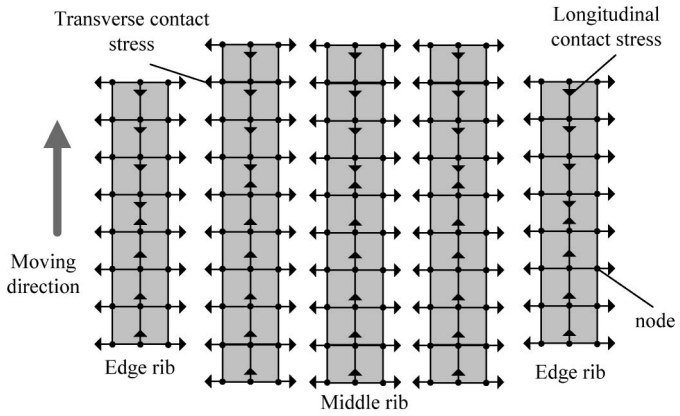

Fig. 4. Schematic illustration of contact stresses under each rib (one tire in dual-tire assembly)

FE Model Validation

The accuracy of FE analysis is affected by mesh dimensions, element definitions, element aspect ratios, complexity of the material models, and the evaluation location. The level of accuracy of the developed FE model was first checked by comparing the FE solutions to a closed-form solution using a layered elastic theory based on general assumptions (e.g., static loading, fully bonded interface conditions, uniform circular contact stress, and linear elastic material behavior) (Al-Qadi and Wang 2009a).

The purpose of this study was to compare the pavement responses under various tire configurations. Table 2 presents the predicted and measured pavement response ratios. The response ratio is the pavement response to the 455 wide-base tire compared to that caused by a dual-tire assembly under the same loading condition. A good agreement of response ratios was achieved for both predicted and measured values for the three sections. Hence, using relatively simple material constitutive models (viscoelastic HMA and elastic aggregate base and subgrade) was thought to be acceptable in this study at a reasonable computation cost.

Pavement Response Analysis

In-Depth Strain Distributions

The pavement responses were calculated under the two tire configurations at 35.5 kN, 690 kPa, and 8 km/h. The tensile and shear strains are the two most critical pavement responses within the HMA layer considered by the mechanistic-empirical design procedure. Figs. 5(a) and 5(b) show the longitudinal tensile strain distributions with depth for section D under two tire configurations at 25°C and 47°C, respectively. The presented tensile strains are located under the middle rib of one tire in a dual-tire assembly where the maximum vertical contact stress exists. As expected, the longitudinal tensile strain distribution is compressive in the upper half of the HMA layer and becomes tensile in the lower part of the layer. The highest tensile strain was obtained at the bottom of the HMA layer at both intermediate and high temperatures. At both temperatures, loading through the wide-base 455 tire resulted in greater longitudinal tensile strains compared to that of the dual-tire assembly.

Figs. 5(c) and 5(d) show the vertical shear strain distributions with depth for section D under two tire configurations at 25°C and 47°C, respectively. At 25°C, the greatest shear strain within the HMA is at the middle of the layer, whereas at 47°C the greatest shear strain is in a shallow depth of the layer (around 20 mm below the surface). The locations of critical shear strain are consistent with the locations where the horizontal tensile strain changes from compression to tension. At high temperature, the high magnitude of shear strain at shallow depth of the HMA layer may initiate near-surface shear cracking or may cause unstable shear flow under repeated vehicular loading. At 47°C, the wide-base 455 tire causes much less vertical shear strain than the dual-tire assembly, while at 25°C, the two tire configurations cause similar vertical shear strains. At an intermediate temperature, 25°C, the shear strain is more controlled by the load-induced bending effect, whereas at high temperature, 47°C, the HMA becomes softer and the effect of localized tire contact stresses (vertical and tangential) become more significant compared to the bending effect. Therefore, at 47°C, the relatively more uniform vertical contact stress and less tangential stress at the edge of the wide-base 455 tire may result in less vertical shear strain at the tire edge compared to the dual-tire assembly.

Stresses and Stains under Various Tire Configurations

Figs. 6(a) and 6(b) show the calculated maximum transverse and longitudinal tensile strains at the bottom of the HMA at 47°C under a dual-tire assembly and a wide-base 455 tire for the three pavement sections. It is clear that the tensile strains decrease as the base layer thickness increases for both tire configurations. The longitudinal tensile strains caused by the wide-base 455 tire are greater than those caused by the dual-tire assembly regardless of base thickness, whereas the transverse tensile strains caused by both tire configurations are relatively similar. Compared to the dual-tire assembly, the wide-base 455 tire causes slightly greater transverse tensile strains in the pavement section having the thinnest base layer but causes slightly less transverse tensile strains in the pavement section having the thickest base layer. These strain differences between the two tire configurations could be a result of the wheel spacing between the tires in the dual-tire assembly; the two tire configurations have similar average contact stress under the same load.

Figs. 6(c) and 6(d) compare the calculated maximum vertical shear stresses and strains at the shallow depth of the HMA layer at 47°C under a dual-tire assembly and a wide-base 455 tire for the three pavement sections. The results show that the wide-base 455 tire causes lower vertical shear stresses and strains than the dual-tire assembly, regardless of base thickness. It is noted that the maximum tensile strains decrease as the base layer thickness increases, whereas the shear strains are insignificantly affected by the base layer thickness. At high temperature, the maximum shear strain is much greater than the maximum tensile strain.

Table 2. Response Ratios Caused by Wide-Base 455 Tire with respect to Dual-Tire Assembly

Sections	A		B		D	
Pavement responses ratios for:	Field	FEM	Field	FEM	Field	FEM
Transverse tensile strain at bottom of HMA	1.12	1.09	1.03	1.01	0.88	0.88
Vertical pressure at bottom of base	1.36	1.24	1.33	1.23	1.16	1.17
Compressive strain on top of subgrade	—	1.21	1.17	1.10	1.10	1.07

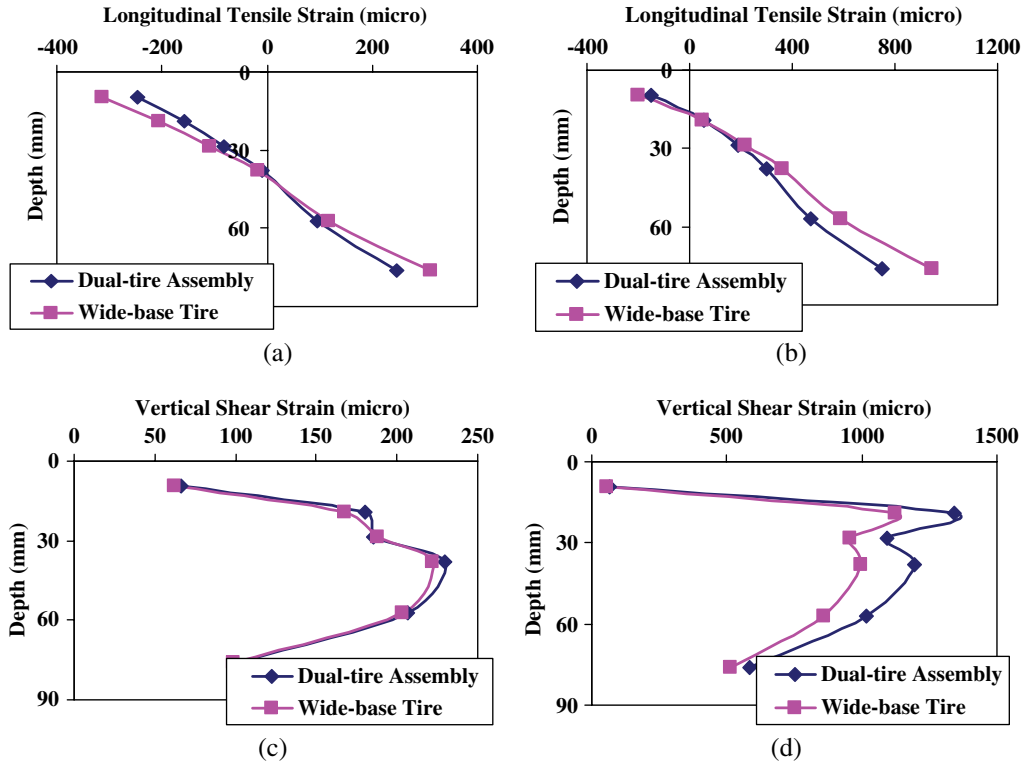

Fig. 5. In-depth strain distributions for: (a) longitudinal tensile strain at 25°C; (b) longitudinal tensile strain at 47°C; (c) vertical shear strain at 25°C; and (d) vertical shear strain at 47°C at section D

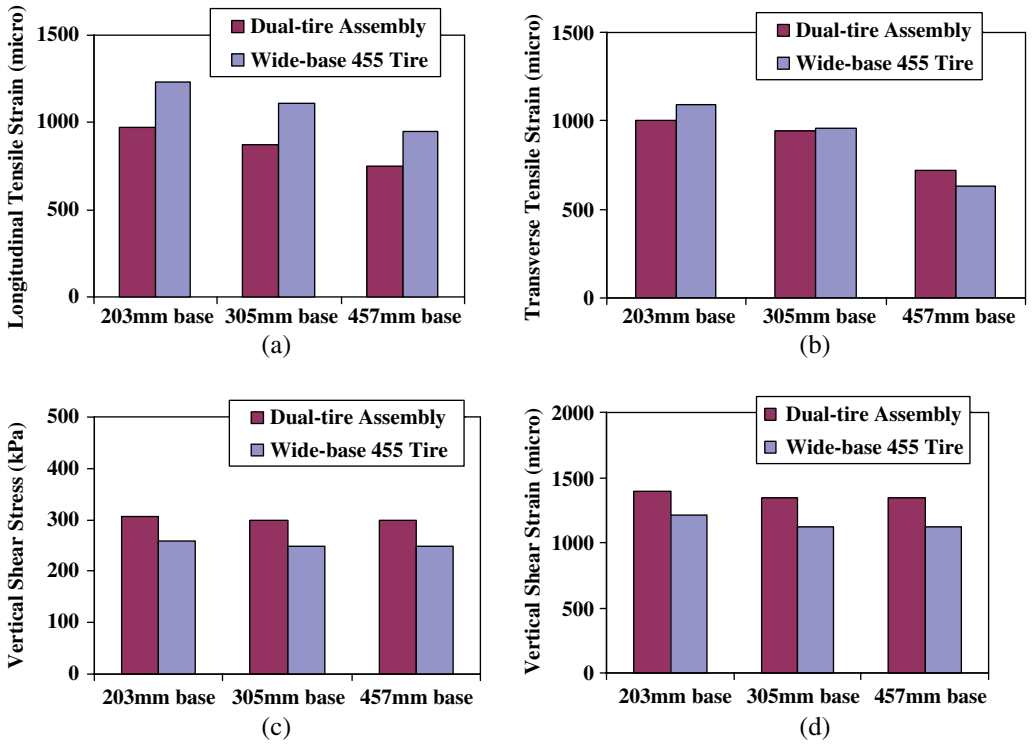

Fig. 6. Comparisons of maximum (a) longitudinal tensile strains; (b) transverse tensile strains; (c) vertical shear stresses; and (d) vertical shear strains under different tire configurations

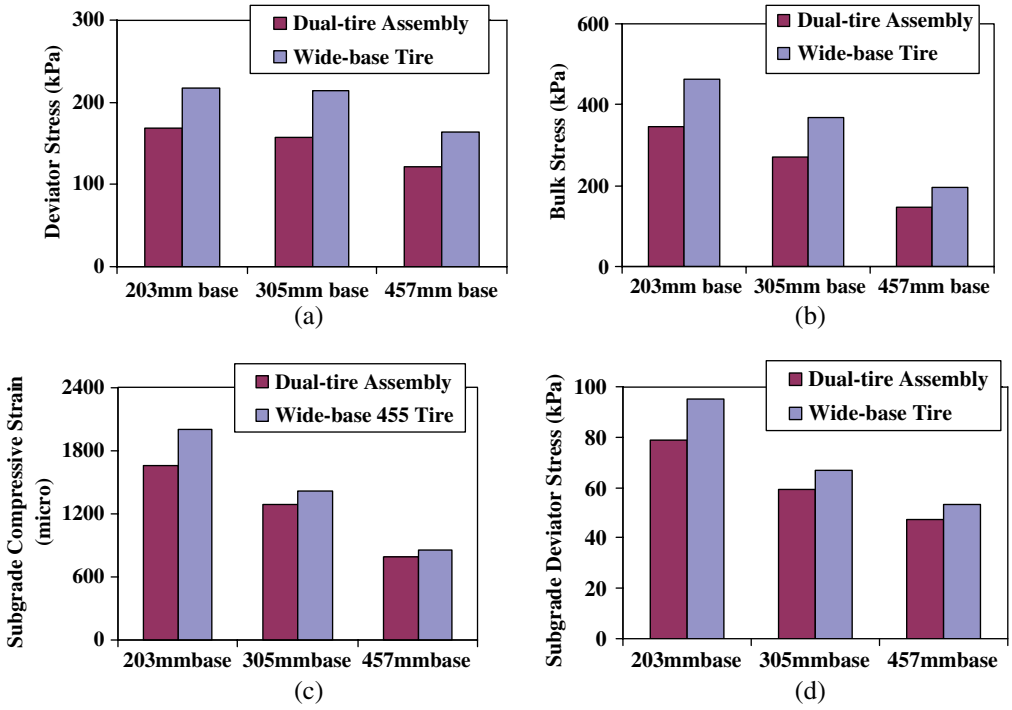

Fig. 7. Comparisons of: (a) base deviator stress; (b) base bulk stress; (c) subgrade compressive strain; and (d) subgrade deviator stress under different tire configurations

This indicates that shape distortion and shear deformation is predominant in the HMA layer at high temperature.

It is documented that the stress state in the middle of the unbound base layer indicates the development of base deformation (Van Gurp and Van Leest 2002). Figs. 7(a) and 7(b) show the bulk and deviator stresses in the middle of the base layer under a dual-tire assembly and a wide-base 455 tire at 47°C for the three pavement sections. The wide-base 455 tire causes greater deviator and bulk stresses in the base layer. A greater deviator stress increases the shear failure potential in the base layer, whereas a greater bulk stress could provide more confinement and restrict the shear failure.

Figs. 7(c) and 7(d) compare the compressive strains and deviator stresses, respectively, on the top of subgrade under a dual-tire assembly and a wide-base 455 tire at 47°C for the three pavement sections. As would be expected, for both tire configurations, the compressive strains and deviator stresses decrease as the base layer thickness increases. The results show that the wide-base 455 tire causes greater compressive strain and deviator stress on top of subgrade than the dual-tire assembly. As the pavement thickness increases, the differences in both strains and stresses between the two tire configurations decrease.

Pavement Damage Models

In this study, pavement damage models (also called transfer functions) were used to provide the relationship between the critical pavement responses and the allowed number of load applications before failure. The main failure mechanisms in each pavement layer and the available damage models for low-volume flexible roads are summarized in the following. The models used here are not mechanistically based—they are empirical-mechanistic models. They are used for the purpose of comparing the impact of the two tire configurations.

Fatigue Cracking of HMA Layer

Tensile strain at the bottom of the HMA layer is thought to be responsible for bottom-up fatigue cracking. High tensile strains are usually caused by heavy loading and/or inadequate structural support from underlying layers. The AASHTO 2002 MEPDG (ARA, Inc. 2004) uses Eq. (5) to determine the number of allowable load applications for fatigue cracking. This method utilizes the initial pavement response and ignores the evolution of strains with damage. However, the introduced error is considered acceptable within the empirical design framework

$$N_f = 0.00432 \cdot k \cdot C \cdot \left(\frac{1}{\varepsilon_t}\right)^{3.9492} \left(\frac{1}{E}\right)^{1.281} \quad (5)$$

where N_f = number of allowed load applications; E = resilient modulus of HMA (in psi); ε_t = tensile strain at pavement surface; C = parameter related to HMA volumetric properties; and k = parameter related to HMA thickness.

Rutting of HMA Layer

Two types of rutting (permanent deformation) may exist in a HMA layer simultaneously: volume reduction caused by traffic densification and aggregate particle movement with a constant volume, or an increasing volume (dilation) caused by shear flow. The general form of HMA rutting models is usually derived from statistical analysis of the relationship between plastic and elastic compressive strains measured from repeated-load uniaxial/triaxial tests. The following transfer function is suggested by the AASHTO 2002 MEPDG (ARA, Inc. 2004):

$$\log\left(\frac{\varepsilon_p}{\varepsilon_r}\right) = -3.7498 + 0.4262\log(N) + 2.02755\log(T) \quad (6)$$

where ε_p = accumulative permanent strain (12.5 mm rutting depth was used as a failure criterion in this study); ε_r = recoverable strain;

N = allowed number of load repetitions corresponding to ε_p; and T = pavement temperature (°C).

Deacon et al. (2002) and Monismith et al. (2006) correlated HMA rutting to shear stresses and shear strains in the HMA layer instead of compressive strain, as shown in Eq. (7). This model was originally developed for Westrack mixes based on repeated simple shear tests at constant height (RSST-CH)

$$\gamma = a \cdot \exp(b\tau_s)\gamma^e n^c \tag{7}$$

where γ = permanent (inelastic) shear strain (12.5-mm rutting depth was used as a failure criterion in this study); γ^e = elastic shear strain; τ_s = corresponding shear stress (in psi); n = number of axle load applications; and a, b, and c are experimentally determined coefficients ($a = 1.262$, $b = 0.05$, and $c = 0.36$ were used in this study).

Permanent Deformation of Unbound Base Layer

Permanent deformation of the base layer is caused by the granular material having insufficient stability owing to heavy loading or poor drainage conditions. This may result in loss of particle-to-particle interlock forces and thus the bearing capacity of base layer (shear failure). It is documented that the stress state in the middle of the unbound base layer indicates the development of deformation (Van Gurp and Van Leest 2002). However, few design methods consider the cumulative permanent deformation or insufficient stability in the granular base layer as critical.

The South African mechanistic design method (SA-MDM) considers the permanent deformation of the base layer. It is related to the ratio of the working stress to the yield strength of the material, considering that high shear stress can extend into the base layer in thin-surfaced pavements for normal traffic loading, Eqs. (8) and (9) (Theyse et al. 1996)

$$F = \frac{\sigma_3[k\tan^2(45+\frac{\phi}{2})-1]+2kc\tan(45+\frac{\phi}{2})}{\sigma_1-\sigma_3} \tag{8}$$

$$N = 10^{(2.605122F+3.480098)} \tag{9}$$

where σ_1 and σ_3 = major and minor principal stresses (compressive stress positive and tensile stress negative); k = constant ($k = 0.95$ for normal moisture condition was used in this study); c = cohesion coefficient; ϕ = angle of internal friction ($c = 0$ and $\phi = 30°$ were used in this study); and N = allowed load applications until failure.

Subgrade Rutting

Subgrade rutting (secondary rutting) is a longitudinal wheel-path depression that occurs when subgrade exhibits permanent deformation caused by compressive or shear stress from repetitive traffic loading. Usually the vertical compressive strain at the top of subgrade is related to subgrade rutting. The Asphalt Institute (AI) (1982) proposed a rutting damage model, based on roadbed soil strain with a maximum threshold of 12.5 mm rutting on subgrade, as follows:

$$N = 1.365 \times 10^{-9}(\varepsilon_v)^{-4.477} \tag{10}$$

where N = allowed load repetitions until failure, and ε_v = maximum vertical compressive strain on top of subgrade.

Damage Ratio between Two Tire Configurations

Using the calculated pavement responses from the FE model and the aforementioned damage models, Table 3 summarizes the calculated damage ratios caused by the 455 wide-base tire with respect to the dual-tire assembly (35.5 kN, 690 kPa, 8 km/h), for, respectively, fatigue cracking, HMA rutting caused by densification, HMA rutting caused by shear, base shear failure, and secondary rutting. The damage ratio for each specific failure mechanism was calculated using Eq. (11). For fatigue cracking, shear failure, and secondary rutting, the allowable number of load applications to failure can be directly predicted from Eqs. (5), (9), and (10), respectively. For HMA rutting caused by densification and shear, the damage ratio is calculated as the ratio of the required load applications between two tire configurations to achieve the same plastic strain [Eqs. (6) and (7)]

$$\mathrm{DR} = N_{w455}/N_{\mathrm{dual}} \tag{11}$$

where DR = damage ratio caused by the 455 wide-base tire with respect to the dual-tire assembly for the considered failure mechanism; N_{w455} = allowable number of load applications to failure for the 455 wide-base tire; and N_{dual} = allowable number of load applications to failure for dual-tire assembly.

The results show that the wide-base 455 tire causes greater fatigue damage, subgrade rutting, and HMA rutting (densification) compared to the conventional dual-tire assembly. For subgrade rutting and HMA rutting resulting from densification, the relative damage ratios between the two tire configurations decrease as the base thickness increases. On the other hand, the wide-base 455 tire causes much less HMA rutting from shear flow than the conventional dual-tire assembly, especially at high temperature. For the base shear failure, the wide-base 455 tire causes greater deviator stress, which increases the failure potential; but it also causes greater confinement stress, which restricts shear failure. The ratio of confinement stress with respect to deviator stress in the base layer is greater under a wide-base 455 tire than under a dual-tire assembly. This reduces the relative potential of shear failure in the unbound base layer.

Combined Damage Ratio

The distress type that allows the fewest number of load applications is expected to cause a pavement's failure. However, the calculation

Table 3. Damage Ratios Caused by Wide-Base 455 Tire with respect to Dual-Tire Assembly

	At 25°C			At 47°C		
Damage mechanism	203-mm base	305-mm base	457-mm base	203-mm base	305-mm base	457-mm base
Fatigue cracking	2.18	2.23	2.41	2.24	1.91	2.50
HMA rutting (densification)	1.77	1.76	1.75	1.53	1.48	1.35
HMA rutting (shear)	0.81	0.68	0.43	0.27	0.22	0.22
Base deformation	0.69	0.92	0.96	0.87	0.92	0.94
Subgrade rutting	1.67	1.31	1.31	2.35	1.55	1.55

of the allowable number of load applications depends significantly on the local calibration factors and material parameters used in the pavement damage models. This could cause the predominant failure type to vary for different loading scenarios. Thus, a combined damage ratio was used to consider the overall effect of different failure mechanisms on pavement serviceability caused by the wide-base 455 tire with respect to the dual-tire assembly.

The combined damage ratio was calculated as a logarithmic damage distribution factor, as shown in Eqs. (12) and (13). The logarithmic distribution function was used to balance the effect of each failure mechanism with respect to the overall damage induced by the tire. This transformation is commonly used in statistics and is recommended when dealing with variables spreading over several orders of magnitude, as is the case presented in this study (Al-Qadi et al. 2005). In the field, even if one failure mechanism is manifested, this does not imply that the other distresses will not occur throughout the pavement service life. The failure mechanisms are progressive and contribute together to degrade the pavement serviceability. For this reason, a combined damage ratio is more appropriate and was, therefore, adopted in this analysis

$$\mathrm{CDR} = a_1 \mathrm{DR}_{\mathrm{fatigue}} + a_2 \mathrm{DR}_{\mathrm{HMA-densification}} + a_3 \mathrm{DR}_{\mathrm{HMA-shear}} + a_4 \mathrm{DR}_{\mathrm{base}} + a_5 \mathrm{DR}_{\mathrm{rutting-subgrade}} \quad (12)$$

$$a_i = \frac{1/\log(N_i)}{\sum_{j=1}^{n} 1/\log(N_j)} \quad (13)$$

where CDR = combined damage ratio caused by the 455 wide-base tire with respect to the dual-tire assembly; $\mathrm{DR}_{\mathrm{fatigue}}$ = damage ratio for fatigue cracking; $\mathrm{DR}_{\mathrm{HMA-densification}}$ = damage ratio for HMA rutting resulting from densification; $\mathrm{DR}_{\mathrm{HMA-shear}}$ = damage ratio for HMA rutting from shear flow; $\mathrm{DR}_{\mathrm{base}}$ = damage ratio for base shear failure; $\mathrm{DR}_{\mathrm{rutting-subgrade}}$ = damage ratio for subgrade rutting; a_1, a_2, a_3, a_4, and a_5 = damage distribution factors for different failure mechanisms; N_i and N_j = allowable number of load applications for different failure mechanisms; and n = total number of considered failure mechanisms ($n = 5$ here).

The calculated combined damage ratios caused by the wide-base 455 tire with respect to the dual-tire assembly are shown in Table 4. In general, the wide-base 455 tire causes 1.12–1.38 times more damage on secondary road pavements, compared to the dual-tire assembly. The combined damage ratios decrease as the base thickness increases. At high temperature, the combined damage ratios are similar or less than those ratios at the intermediate temperature. The impact of the wide-base 455 tire on interstate highways (thick pavement), it should be noted, is less than that on secondary roads. The combined damage ratios were found to be close to unity in thick pavement (Al-Qadi and Wang 2009b).

Use of Damage Ratio in Road Pricing and Pavement Design

The calculated combined damage ratio between two tire configurations represents the equivalent number of passes of the dual-tire assembly to cause the same amount of damage as one pass of the wide-base 455 tire. Thus, the ratio can be used to compare the costs induced by the two tire configurations if the load equivalency factor (LEF) and the reference cost are known. For example, the Illinois Department of Transportation's (IDOT's) Truck Size and Weight Report (2006) states that the pavement cost (new construction plus rehabilitation) per equivalent single axle load (ESAL)-mile with dual-tire assembly is \$0.508 for local roads. Using the AASHTO LEF, the pavement cost per mile per pass caused by the dual-tire assembly at 35.5 kN would be $\$0.508 \times 0.61 = \$0.31$. Then the pavement cost per mile per pass caused by the wide-base 455 tire at the same load would be \$0.31 multiplied by the combined damage ratio. The estimated pavement cost provides state pavement agencies a basis for implementing appropriate load regulations and road pricing for trucking operations using wide-base tires.

The damage ratio can also be used to convert the number of axles with wide-base tires to the number of axles with dual-tire assembly in pavement design practice. If the pavement is designed based on a specific failure type using a mechanistic-empirical approach, the damage ratio corresponding to the specific failure mechanism can be used. For designers using the MEPDG software, the input traffic data would be the summation of the actual traffic using dual-tire assembly and the equivalent traffic that is converted from the passes of wide-base tires using the combined damage ratio. If the pavement is designed in accordance with the AASHTO design guidelines (AASHTO 1993), the LEF for the corresponding wide-base tires can be calculated as: LEF for wide-base tires at a given axle load is equal to AASHTO LEF for the axle load multiplied by the combined damage ratio obtained from this study. The aforementioned ratios may be used for secondary roads only. Other values may need to be used for primary flexible pavements (Al-Qadi and Wang 2009b).

Table 4. Combined Damage Ratio between Two Tire Configurations

Design temperature (°C)	Base thickness (mm)		
	203	305	457
25	1.37	1.29	1.24
47	1.38	1.12	1.14

Conclusions

In this study, a 3D FE model was built to predict pavement responses to loading applied by various tire configurations on secondary road pavements. The 3D FE model was validated using the strain measurements from accelerated pavement testing. The impact of wide-base tires on secondary road pavement damage was then analyzed using available damage models. The results were compared to the damage from conventional dual-tire assemblies. The results show that the new generation of wide-base tire causes greater fatigue damage, subgrade rutting, and HMA rutting (densification) compared to conventional dual-tire assembly when carrying the same load. On the other hand, the new wide-base tire causes less HMA rutting (shear) and base shear failure potential than the conventional dual-tire assembly. These damage ratios vary with base layer thickness, HMA temperature, and possibly, loading. The study found that wide-base tires' impact on secondary road pavement damage depends on roads' predominant failure mechanisms. Thus, a combined damage ratio was used to consider the overall effect of various failure mechanisms on pavement serviceability. The calculated combined damage ratio can be used for road pricing and in pavement design practice when wide-base tires are used.

Acknowledgments

The results presented in this paper are based on the NEXTRANS Center Project No. 008IY01, conducted in cooperation with the Illinois Center for Transportation (ICT). The earlier work by J. Yoo and M. A. Elseifi is acknowledged. The computing support

provided by the National Center for Super Computing Applications (NCSA) at the University of Illinois at Urbana-Champaign is greatly appreciated. The contents of this paper reflect the view of the writers, who are responsible for the facts and the accuracy of the data presented here. The contents do not necessarily reflect the official views or policies of the NEXTRANS, FHWA, ICT, or IDOT. This paper does not constitute a standard, specification, or regulation.

References

AASHTO. (1993). "AASHTO guide for design of pavement structures." Washington, DC.

ABAQUS version 6.7 [Computer software]. Hibbitt, Karlsson, and Sorenson, Inc., Pawtucket, R.I.

Akram, T., Scullion, T., Smith, R. E., and Fernando, E. G. (1992). "Estimating damage effects of dual versus wide-base tires with multidepth deflectometers." *Transp. Res. Rec.*, 1355, 59–66.

Al-Qadi, I. L., and Elseifi, M. a. (2007). "New generation of wide-base tires: impact on trucking operations, environment, and pavements." *Transp. Res. Rec.*, 2008, 100–109.

Al-Qadi, I. L., and Wang, H. (2009a). "Full-depth pavement responses under various tire configurations: Accelerated pavement testing and finite element modeling." *J. Assoc. Asphalt Paving Technol.*, 78, 645–680.

Al-Qadi, I. L., and Wang, H. (2009b). "Evaluation of pavement damage due to new tire designs." *Research Rep. ICT-09-048*, Illinois Center for Transportation, Rantoul, IL.

Al-Qadi, I. L., Loulizi, A., Janajreh, I., and Freeman, T. E. (2002). "Pavement response to dual tires and new wide-base tires at same tire pressure." *Transp. Res. Rec.*, 1806, 38–47.

Al-Qadi, I. L., Tutumluer, E., Dessouky, S. H., and Kwon, J. (2007). "Effectiveness of geogrid-reinforcement in flexible pavements: A full-scale testing." *Final Report to Tensar Earth Technologies, Inc.*, University of Illinois, Urbana-Champaign, IL.

Al-Qadi, I. L., Wang, H., Yoo, P. J., and Dessouky, S. H. (2008). "Dynamic analysis and in situ validation of perpetual pavement response to vehicular loading." *Transp. Res. Rec.*, 2087, 29–39.

Al-Qadi, I. L., Yoo, P. J., Elseifi, M. A., and Janajreh, I. (2005). "Effects of tire configurations on pavement damage." *J. Assoc. Asphalt Paving Technol.*, 74, 921–962.

Ang-Olson, J., and Schroeer, W. (2002). "Energy efficiency strategies for freight trucking: potential impact on fuel use and greenhouse gas emission." *Transp. Res. Rec.*, 1815, 11–18.

Applied Research Associates, Inc. (ARA). (2004). "Development of the 2002 guide for the design of new and rehabilitated pavements." National Cooperative Highway Research Program (NCHRP) Proj. No. 1-37A, Transportation Research Board, Washington, DC.

Asphalt Institute (AI). (1982). "Research and development of the Asphalt Institute's thickness design manual (MS-1)," *Research Rep. 82-1*, 9th Ed., College Park, MD.

Bathe, K. J. (1996). *Finite element procedures in engineering analysis*, Prentice-Hall, Upper Saddle River, NJ.

Bonaquist, R. (1992). "An assessment of the increased damage potential of widebase single tires." *Proc, 7th Int. Conf. on Asphalt Pavements*, Vol. 3, Int. Soc. for Asphalt Pavements, Lino Lakes, MN, 1–16.

Chopra, A. K. (2001). *Dynamics of structures*, 2nd Ed., Prentice-Hall, Upper Saddle River, NJ.

COST Action 334. (2001). "Effects of wide single tires and dual tires." European Cooperation in Science and Technology (COST), Brussels, Belgium.

Deacon, J. A., Harvey, J. T., Guada, I., Popescu, L., and Monismith, C. L. (2002). "Analytically based approach to rutting prediction." *Transp. Res. Rec.*, 1806, 9–18.

De Beer, M., Fisher, C., and Jooste, F. J. (2002). "Evaluation of nonuniform tire contact stresses on thin asphalt pavements." *Proc., 9th Int. Conf. on Asphalt Pavements (ICAP 2002)* (CD-ROM), Int. Soc. for Asphalt Pavements, Lino Lakes, MN.

Drakos, C., Roque, R., and Birgisson, B. (2001). "Effects of measured tire contact stresses on near surface rutting." *Transp. Res. Rec.*, 1764, 59–69.

Huhtala, M., Philajamaki, J., and Pienimaki, M. (1989). "Effects of tires and tire pressures on road pavements." *Transp. Res. Rec.*, 1227, 107–114.

Illinois Department of Transportation (DOT). (2006). "Truck size and weight report." Springfield, IL

Kim, D., Salgado, R., and Altschaeffl, A. G. (2005). "Effects of supersingle tire loadings on pavements." *J. Transp. Eng.*, 131(10), 732–743.

Monismith, C. L., Popescu, L., and Harvey, J. T. (2006). "Rut depth estimation for mechanistic-empirical pavement design using simple shear test results." *J. Assoc. Asphalt Paving Technol.* (CD-ROM), 75, 1294–1338.

Myers, L. A., Roque, R., Ruth, B. E., and Drakos, C. (1999). "Measurement of contact stresses for different truck tire types to evaluate their influence on near-surface cracking and rutting." *Transp. Res. Rec.*, 1655, 175–184.

Organization for Economic Cooperation and Development (OECD). (1992). *Dynamic loading of pavements: Road transport research*, Paris.

Park, S. W., and Kim, Y. R. (1999). "Interconversion between relaxation modulus and creep compliance for viscoelastic solids." *J. Mater. Civ. Eng.*, 11(1), 76–82.

Park, D., Martin, A. E., and Masad, E. (2005). "Effects of nonuniform tire contact stresses on pavement response." *J. Transp. Eng.*, 131(11), 873–879.

Perdomo, D., and Nokes, B. (1993). "Theoretical analysis of the effects of wide-base tires on flexible pavements using CIRCLY." *Transp. Res. Rec.*, 1388, 108–119.

Pierre, P., Dore, G., and Vagile, L. (2003). "Characterization and evaluation of tire-roadway interface stresses." *Rep. No. GCT-03-03*, Québec Ministry of Transport, Montréal.

Priest, A. L., Timm, D. H., and Barrett, W. E. (2005). "Mechanistic comparison of wide-base single vs. standard dual tire configurations." *Rep. 05-03*, National Center for Asphalt Technology (NCAT), Auburn, AL.

Siddharthan, R. V., Krishnamenon, N., El-Mously, M., and Sebaaly, P. E. (2002). "Investigation of tire contact stress distributions on pavement response." *J. Transp. Eng.*, 128(2), 136–144.

Theyse, H. L., De Beer, M., and Rust, F. C. (1996). "Overview of the South African mechanistic pavement design analysis method." *Transp. Res. Rec.*, 1539, 6–17.

Van Gurp, C., and Van Leest, A. J. (2002). "Thin asphalt pavements on soft soil." *Proc., 9th Int. Conf. on Asphalt Pavements* (CD-ROM), Int. Soc. for Asphalt Pavements, Lino Lakes, MN.

Wang, H., and Al-Qadi, I. L. (2009). "Combined effect of moving wheel loading and three-dimensional contact stresses on perpetual pavement responses." *Transp. Res. Rec.*, 2095, 53–61.

Yoo, P. J., and Al-Qadi, I. L. (2007). "Effect of transient dynamic loading on flexible pavements." *Transp. Res. Rec.*, 1990, 129–140.

Yoo, P. J., and Al-Qadi, I. L. (2008). "Truth and myth of fatigue cracking potential in hot-mix asphalt: Numerical analysis and validation." *J. Assoc. Asphalt Paving Technol.*, 77, 549–590.